

# ANALYSIS OF A HIGH-PRESSURE MULTISTAGE AXIAL COMPRESSOR AT OFF-DESIGN CONDITIONS WITH COARSE LARGE EDDY SIMULATIONS

*J. de Laborderie - F. Duchaine - L. Gicquel*

CFD Team - CERFACS  
42 avenue G. Coriolis  
31057 Toulouse, FRANCE  
jerome.de.laborderie@cerfacs.fr

## ABSTRACT

This paper aims at evaluating Large Eddy Simulations (LES) for the prediction of the performance line and flow at off-design conditions in a multistage high-pressure compressor. A coarse and an intermediate grid are specifically investigated, since their associated computational cost appears affordable in an industrial context. Several operating conditions of the 3.5 stages high-pressure compressor CREATE are simulated, then results are compared to experimental data and to an existing URANS simulation. Both grids yield iso-speed performance lines close to experimental measurements, but only the intermediate one is able to correctly predict the experimental point at lowest mass flow rate. The unstable regime is specifically investigated in the last stage of the intermediate grid, showing the presence of rotating instabilities. Their amount and spinning velocity are similar to experimental observations and previous URANS results. Hence coarse LES appears as an interesting tradeoff for off-design predictions of flow in a multistage compressor.

## KEYWORDS

LES, AXIAL COMPRESSOR, OFF-DESIGN

## NOMENCLATURE

$f$  frequency

$h/H$  duct height

$m$  circumferential mode

$N_R$  number of rotor blades

$N_S$  number of stator vanes

$P_t$  total pressure

$\Omega$  rotational velocity

$\Pi$  total pressure ratio

## INTRODUCTION

In the design process of a multistage compressor, an accurate prediction of performances and flow field is critical at off-design conditions and low mass flow rate. Indeed, this directly drives the expected surge margin thereby greatly influencing the compressor efficiency and operating range. At low mass flow rate, a compressor enters an unstable regime that has been under investigation over several decades to improve general understanding of its inception and

development (Day, 2016). Depending upon the configuration, this regime may lead to local or global modifications of the flow, referred as stall, and ultimately to surge, characterized by mass flow reversal. Numerical predictions of stall and surge in compressors are challenging since the system is unstable by nature, and the flow is expected to be more complex than at nominal conditions. Nevertheless CFD is definitely a way to bring further understanding and control of this unstable regime (Day, 2016).

Among the existing studies, the 3.5 stages axial high-pressure compressor CREATE has recently been the object of test campaigns to characterize its behavior at off-design conditions. Courtiade and Ottavy (2013) observed appearance of 18 instabilities rotating at 57% of shaft speed, that transform into stall cells and finally lead to surge. Crevel et al. (2014) performed numerical studies of CREATE at off-design conditions, using a URANS approach on two configurations, one being the compressor alone and the other one being the compressor embedded in its test rig. In the first case, 24 rotating instabilities at 79.2% of the shaft speed were noticed. In the second case, only 16 rotating instabilities at 80.6% of the shaft speed were captured. It was also shown that the plenums located upstream and downstream the compressor need to be accounted for to simulate a full surge cycle. Recently, on a different version of CREATE, the URANS simulation of Schreiber et al. (2016) showed 32 rotating instabilities at 72% of shaft speed at a low mass flow rate operating point. All these simulations were performed over an azimuthal sector of the compressor, hence enforcing the amount of instabilities to be a multiple of the circumferential periodicity.

It is commonly admitted by the turbulent modeling community as well as in CFD developments that Large Eddy Simulation (LES) has the potential to become the numerical flow simulation method that can provide breakthroughs in the design and understanding of future aeroengine components (Tucker, 2011). If this has already been shown for some parts of the engine at given operating conditions, the computational cost of LES still prevents to fully compute a compressor performance map. Recently, LES of the full CREATE compressor has been performed at nominal operating conditions (de Laborderie et al., 2016), using a wall law approach. Among the three grids used, the most refined one contains more than one billion cells. Results in terms of global performances and averaged radial profiles were promising with respect to experimental data. In an attempt to further evaluate LES of compressors, the objectives consist here to assess LES as a tool to obtain a compressor performance map based on the aforementioned preliminary computations, and to analyze the flow at low mass flow rates.

The present paper is structured as follows. The experimental facility is briefly introduced, then the numerical method and its application to the multistage compressor CREATE are described. Results are then analyzed in terms of global aerodynamic performances and flow fields. Finally, an analysis of instabilities expected to occur at off-design conditions in this machine is performed to evaluate the capability of LES.

## **EXPERIMENTAL FACILITY**

The multistage research compressor CREATE (Compresseur de Recherche pour l'Etude des effets Aerodynamiques et Technologiques), designed by Safran Aircraft Engines and operated at LMFA (Ecole Centrale de Lyon, France), is the machine chosen for the present study. The configuration corresponds to the CREATE2bis geometry. CREATE is a high-pressure high-speed 3.5 stages axial compressor, representative of high-pressure compressor median-rear blocks in modern turbofan engines. Figure 1 presents a view of the meridian cut of the compressor, showing a variable Inlet Guide Vane (IGV), three rotors (R1, R2, R3) and three stators (S1, S2, S2).

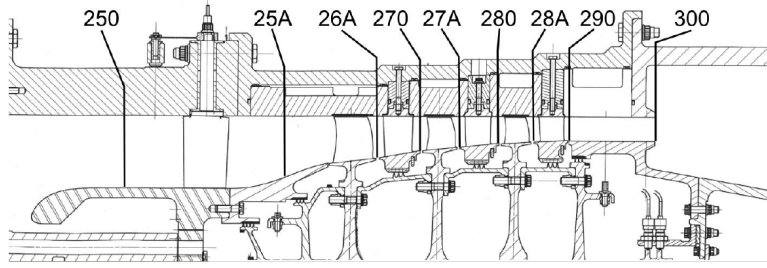


Figure 1: **Meridian cut of the compressor CREATE (Ottavy et al., 2012).**

Row	IGV	R1	S1	R2	S2	R3	S3
For $2\pi$	32	64	96	80	112	80	128
For $2\pi/16$	2	4	6	5	7	5	8

Table 1: **Number of blades in each row of CREATE.**

The number of blades per row, noted in Table 1, has been chosen in the design process so that the compressor has a natural circumferential periodicity of  $2\pi/16$ . The casing outer diameter is constant throughout the machine. The design shaft speed is 11543 rev./min., inducing a 0.92 inlet Mach number at the tip of R1. Hence the flow is slightly transonic in the first rotor and fully subsonic in the other rows. The Reynolds number based on the chord of R1 is around  $10^6$ .

## NUMERICAL SET-UP

### Numerical method

TurboAVBP is the LES code coupling strategy proposed by CERFACS for turbomachinery flows. It relies on the external coupling of separate instances of the AVBP LES solver (Schonfeld and Rudyard, 1999). Within each AVBP instance, the filtered unsteady compressible Navier-Stokes equations are solved on unstructured grids. These equations describing the mass, momentum and energy conservation, can be written as:

$$\frac{\partial \mathbf{W}}{\partial t} + \nabla \cdot \mathcal{F} = 0. \quad (1)$$

$\mathbf{W}$  contains the conservative variables  $(\rho, \rho \mathbf{U}, \rho E)$  and  $\mathcal{F}$  is the flux tensor. The latter is decomposed into a convective part  $\mathcal{F}^c(\mathbf{W})$  and a viscous part  $\mathcal{F}^v(\mathbf{W}, \nabla \mathbf{W})$ . The fluid is considered as a perfect gas. The unresolved turbulent contributions are included in the viscous flux  $\mathcal{F}^v$  with a sub-grid scale model, using the turbulent viscosity approach. To be consistent between simulations that use wall functions, the Smagorinsky sub-grid scale model is employed (Smagorinsky, 1963). For computational cost reasons, the finite volume Lax-Wendroff scheme, second-order accurate in space and time, is preferred (Lax and Wendroff, 1964).

The external coupling of several AVBP instances is performed with the OpenPALM coupler (Duchaine et al., 2015), co-developed by ONERA and CERFACS. Each computational domain with its own grid velocity is attributed to a dedicated instance. The transfer of information between these domains is realized with the overset grid method MISCOG (Multi Instance Solver Coupled through Overlapping Grids), proposed and detailed by Wang et al. (2014). The working principle of MISCOG consists in the exchange, at each time step, of the conservative variables at nodes belonging to cells that overlap around the interfaces. As the nodes in each

domain are not coincident at every time step, an interpolation of the conservative variables is carried out. MISCOG was originally developed with a spatially second order accurate interpolation and has recently been extended with a third order accurate interpolation, based on the Hermite polynomial technique. This overset grid approach is not fully conservative (Wang et al., 2014). However, for the CREATE simulations presented in this paper, the relative mass and energy errors across each interface are less than 0.1% and 0.2% respectively. In moving domains, the mesh movement is performed with the ALE method (Moureau et al., 2005) and the equations are solved in the absolute reference frame.

### **Computational domain**

The computational domain for the TurboAVBP simulations, shown in Fig. 2, corresponds to an azimuthal sector of one sixteenth of the machine, following its natural periodicity (see Tab. 1). This choice forces the periodicity of the flow at the lateral boundaries, which naturally infers a limitation to simulate the actual flow developing in the machine. At off-design conditions, structures that may develop are therefore constrained by this periodicity. This approach is driven by the huge computational cost that a 360 degree simulation would represent. It prevents to reach the actual flow at low mass flow rates, but has already been successfully used by Crevel et al. (2014) for instance, for the same compressor. Indeed, structures predicted by the simulation could be compared to experimental observations.

The TurboAVBP strategy consists here in attributing one instance (AVBP01) to the fixed domain containing the stator rows, and the other instance (AVBP02) to the moving domain containing the rotor rows, since all the rows rotate at the same speed. Several technological effects are accounted for in the simulations, including the actual tip clearances between the three rotors and the casing, as well as the recirculating cavity with a labyrinth seal below the first stator. As shown in Fig. 2, 6 overlapping MISCOG interfaces are present within the computational domain. It has recently been shown that successively adding MISCOG interfaces does not deteriorate the numerical properties of TurboAVBP (de Laborderie et al., 2016).

The inlet of the domain corresponds to the experimental plane 250 of Fig. 1, located 1.3 axial Inlet Guide Vane (IGV) chord upstream of the IGV, where the measured mean total pressure and total temperature radial profiles are imposed. No turbulence is injected through this inlet. Plane 300 is the outlet of the domain, located 2.3 axial S3 vane chords downstream of the third stator, where a target static pressure is imposed. To ensure no reflection of acoustic waves at the inlet and at the outlet of the domain, Navier-Stokes Characteristic Boundary Conditions (NSCBC) are employed (Poinsot and Lele, 1992). It has recently been shown that a characteristic outlet boundary condition, including transverse terms, is particularly suited for turbomachinery flows since it allows the radial equilibrium to naturally take place around the target static pressure value (Koupper et al., 2014). Moreover for an axial compressor at low mass flow rate, a small variation of exit pressure leads to a relatively large variation of mass flow. According to Vahdati et al. (2005), a fixed outlet pressure has to be avoided in this case because of its stiffness. The present outlet NSCBC fulfills this requirement as the exit pressure is imposed with some relaxation. It has been checked that this condition allows a significant variation of the outlet mass flow. A two-variable exit condition, modeling a throttle condition, is often used for off-design simulations, e.g. by Crevel et al. (2014). This condition, coupled to NSCBC formalism, could be evaluated in AVBP in the future. An adiabatic law of the wall condition is imposed to the whole set of walls present in the simulation, i.e. blades, hub and tip casings. This wall function is based on a two-layer approach, valid for a flat plate without any pressure gradient.

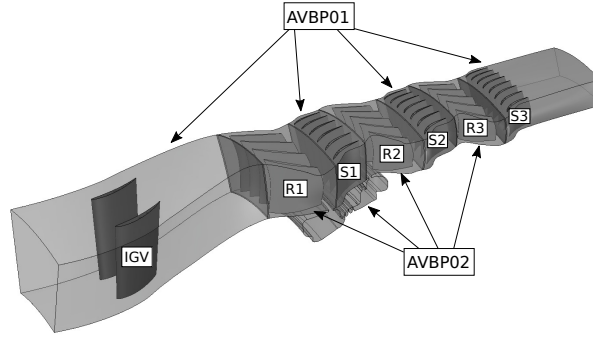


Figure 2: **Computational domain for TurboAVBP.**

Grids	M1	M2	M3
Nb. cells ( $\times 10^6$ )	88	194	1032
Nb. prisms layers on blades	0	3	10
Nb. cells layers in rotor tip gaps	3	6	20
Max. $y^+$ on blades	500	100	40
Cut-off frequency (kHz)	214	256	510
CPU cost per revolution (kh)	17	165	2020

Table 2: **Main properties of the grids.**

It is thus a limitation for the simulations, for which near-wall flow is 3D and possibly detached.

### Mesh and cost of simulations

Three fully unstructured grids have been generated and their main features are gathered in Tab. 2. M1 is a fully tetrahedral grid whereas several layers of prisms on all the blades and vanes are present in M2 and M3. The prismatic cells allow to decrease the distance to the wall of the first node inside the flow while limiting the additional amount of cells. Note that with more than one billion of cells, the M3 grid agrees with the expected order of magnitude of a LES grid for industrial compressors at  $Re \approx 10^6$  (Tucker, 2011). As reported in Tab. 2, the time-averaged normalized distance to the wall  $y^+$  is less than 100 and 40 for M2 and M3 respectively, allowing a relevant use of a law of the wall. This value appears too large for M1 to expect proper near-wall flow physics. The cut-off frequencies are large enough to ensure a proper grid resolution of the unsteady phenomena studied.

The CPU cost, directly related to the mesh size and the time step, increases from one order of magnitude from M1 to M2 and M2 to M3 (see Tab. 2). For M1 and M2, costs of one compressor revolution are affordable and similar to current simulations that can be performed in industry. For M3, the huge cost associated with one revolution prevents simulating several revolutions, that are needed to reach an iso-speed performance line and to study off-design conditions.

## OVERALL ANALYSIS

### Global aerodynamic performances

Recently, TurboAVBP simulations of CREATE have been performed at nominal operating conditions, for the three grids mentioned above (de Laborderie et al., 2016). It has been shown,

using available experimental data, that global performances were correctly predicted for each grid, as well as radial profiles of total pressure and temperature at each inter-row section (see Fig. 1). It has been noticed though that only the most refined grid (M3) gives an accurate prediction close to the casing, where successive interactions of wakes and tip clearances flows are responsible for complex flow physics.

Going beyond the study at nominal conditions, the present objective consists first in the evaluation of the capability of LES to predict the performance map of a multistage compressor. This implies the simulation of several operating conditions for each grid. It has already been noticed that for a given operating point, two wheel revolutions are needed to stabilize the mass flow, and only then can statistics be recorded during two further wheel revolutions. The chosen convergence criterion relies on the variation of averaged mass flow, found to be less than 0.1% between these last two revolutions. Due to the computational cost of one revolution for M3 (see Tab. 2), simulating several operating points is still out-of-reach for the most refined grid. As the cost for one revolution is affordable for M1 and M2, the present paper focuses on these two grids.

Figure 3 presents the performance curve of CREATE at nominal speed in terms of total pressure ratio. The values are normalized by the experimental quantities at the nominal point. The experimental data are shown with their uncertainties evaluated by Ottavy et al. (2012). LES results, represented with circles for M1 and squares for M2, are post-processed consistently with measured data. Namely the total pressure ratio is defined as:

$$\Pi = \frac{\overline{P_{t,o}}}{P_{t,i}}, \quad (2)$$

where  $P_{t,i}$  is the time-averaged total pressure in plane 250 at one point at mid-height of the duct. In the test rig, the output total pressure  $\overline{P_{t,o}}$  is the arithmetic average of measurements over 30 probes located in plane 300, equally distributed on 6 rakes over the full annulus. For LES,  $\overline{P_{t,o}}$  is defined as:

$$\overline{P_{t,o}} = \frac{1}{N} \sum_{k=1}^N P_{t,o,k}, \quad (3)$$

where the 15 numerical probes  $k$  are distributed along three lines in the azimuthal direction over the  $2\pi/16$  sector. Their radial locations match the positions of experimental probes.

In addition to the uncertainties linked to errors in measurements chains, Schreiber et al. (2016) have recently quantified some discrepancies between experimental and numerical studies of CREATE. First, the geometry of the computational domain is simplified as it does not account for leakages at hub and casing between each row, except below S1. Second, the eight struts supporting the hub upstream of plane 250 (see Fig. 1) are not included in the domain. The estimated offsets created by these discrepancies are estimated to 3.8% on the mass flow and to 0.1 total pressure ratio point. Using these estimations, the LES predictions are found within the correct range relatively to the measurements.

For LES, the operating points were obtained by varying the pressure imposed at the outlet. As explained above, each point corresponds to a simulation lasting at least four revolutions to ensure the mass flow stabilization. It can be noticed that shapes and levels of both LES curves are rather close to the experimental iso-speed line. More precisely, the grid refinement from M1 to M2 allows the performance curve to be closer to measured data in the low mass flow region.

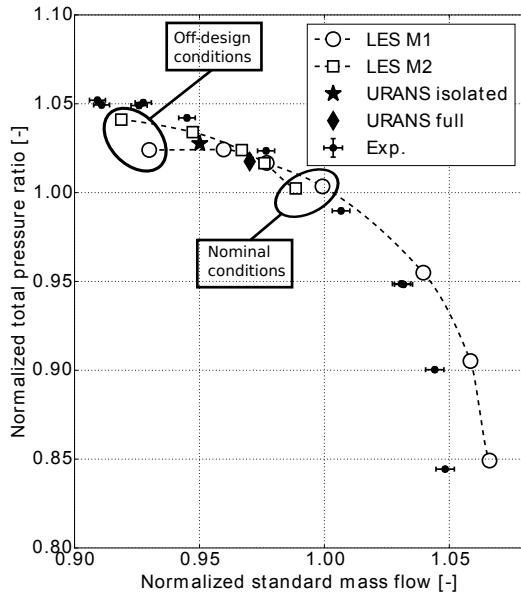


Figure 3: **Performance curve of CREATE. Comparison of LES predictions with experimental data (Ottavy et al., 2012) and URANS results (Crevel et al., 2014).**

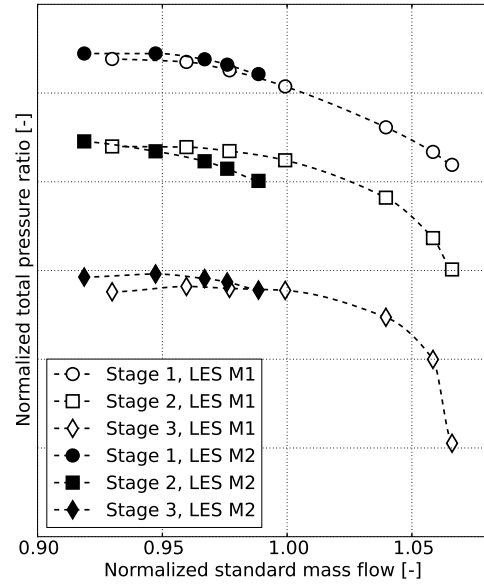


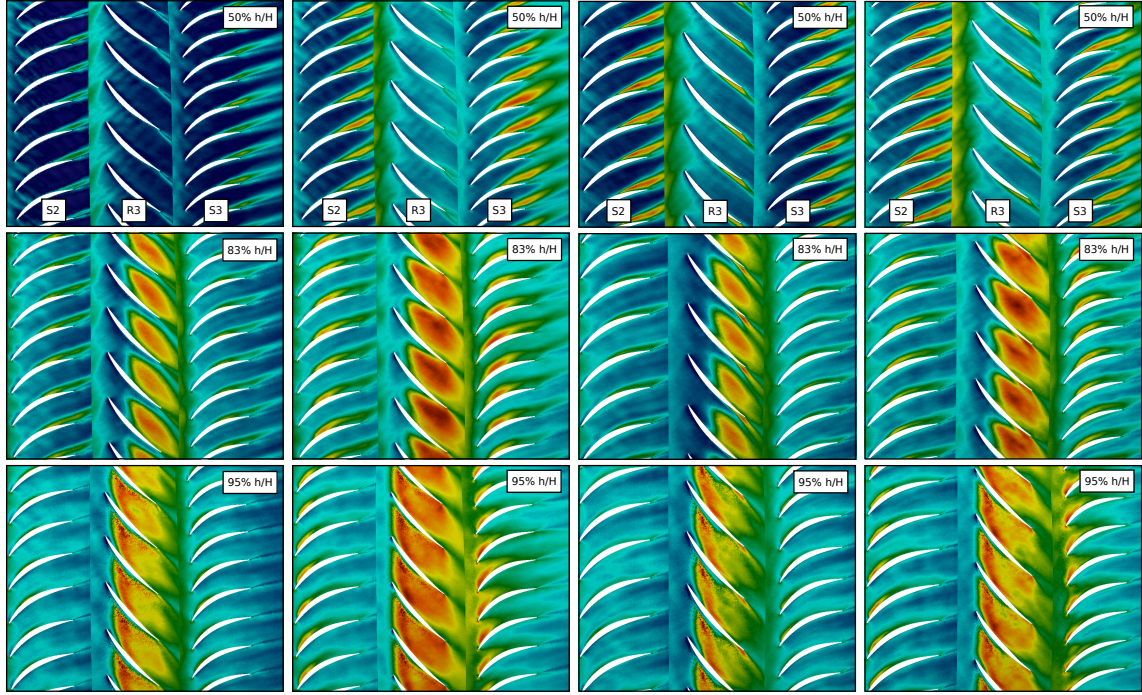
Figure 4: **LES predictions of performance curves of each stage of CREATE.**

The grid refinement effort from M1 to M2 mainly concerns near wall regions of blades and tip clearances of rotors. An improved prediction of flow dynamics and losses is thus expected in these zones, that reveals to be critical for global performance prediction. The lowest mass flow operating point for M1 has been obtained for a variation of 3.2% of back pressure relatively to nominal conditions. It has furthermore been verified that an increase of 0.3% of back pressure from this last point leads grid M1 to mass flow reversal, or numerical surge. For M2 grid, the lowest mass flow conditions correspond to a variation of 5.3% of outlet pressure respectively to nominal conditions. The grid refinement is thus crucial to get stable operating conditions at lower mass flow rate, approaching the experimental stability limit.

URANS results from Crevel et al. (2014) are added to Fig. 3 to be compared with the present simulations. The star symbol corresponds to the simulation on the compressor alone, whereas the diamond refers to the compressor embedded in its test rig. These two URANS operating points, specifically defined to study off-design conditions, match well both LES performance curves. Further comparisons of LES and URANS are thus relevant.

In the following, two specific sets of points will be surveyed. They are circled in Fig. 3. The off-design conditions for M1 and M2 correspond to the lowest mass flow rate obtained for both grids. The nominal operating points will be used to analyze the change in physics between design and off-design conditions.

Figure 4 presents the performance curve of each stage of CREATE for both grids. The total pressure has been time and spatially averaged upstream and downstream each successive stage. This representation is useful to determine if a particular stage is restrictive for the global stability limit of the whole compressor. For both grids, it is seen that the slope of the total



(a) M1, nominal point. (b) M1, off-design point. (c) M2, nominal point. (d) M2, off-design point.

**Figure 5: Axial velocity fluctuations (RMS) in the rear 1.5 stage. Normalized color scale is the same for all plots, going from zero (blue) to one (red).**

pressure ratio curves of stages 1 and 2 is monotonic up to the lowest mass flow point. This is not the case for stage 3, for which a change in the slope occurs at 0.96 normalized mass flow for M1 and 0.95 for M2. This means that stage 3 has reached unstable operating conditions for the off-design points, whereas stages 1 and 2 are still working in their stable operating range. This is in accordance with previous experimental (Courtiade et al., 2013) and numerical (Crevel et al., 2014) studies on this compressor. That is why the following analysis will mainly focus on stage 3.

### Flow field in blade-to-blade planes

LES simulations are first analyzed in terms of flow fields in blade to blade planes. Figure 5 corresponds to the axial velocity fluctuation at three duct heights ( $h/H$ ), for M1 and M2 grids, at both specific operating points: nominal and off-design (see Fig. 3). For each grid, fluctuations have larger amplitudes at off-design than at nominal conditions. At 50% and 83%  $h/H$ , large flow separations can be seen on S2 and S3 vanes at off-design, whereas the flow seems to stay attached in R3. At 95%  $h/H$ , the tip clearance flow above rotor 3 is clearly visible as it is responsible for large fluctuations in the rotor blade passages. In both grids, the path of the tip leakage vortex can be hinted: it stays inside the blade passage at nominal conditions, whereas it is pushed up towards the inlet of the passage at off-design conditions. This expected behavior shows that these under-resolved LES are able to qualitatively reproduce flow modifications from nominal to off-design conditions.

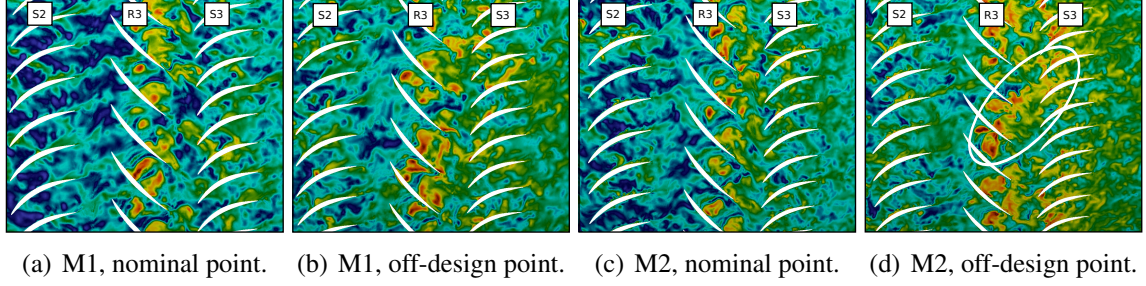


Figure 6: **Instantaneous entropy field at 83% of duct height. Normalized color scale is the same for all plots, going from zero (blue) to one (red).**

### ANALYSIS OF INSTABILITIES

As reported by Day (2016), rotating instabilities may appear in multistage compressors operating at low mass flow rates, before rotating stall regimes. They are located close to rotor blade tips with large clearances, have a spinning velocity lower than the rotational speed, and time varying properties (frequency, amplitudes...). As recalled in the introduction, previous experimental and numerical investigations of CREATE have highlighted the presence of these rotating instabilities, in the rear part of the compressor. Figure 6 presents the instantaneous entropy at 83%  $h/H$ , in S2, R3 and S3, for both grids and both operating points. At nominal conditions, some local spots of high entropy are visible in the rotor channels (Figs. 6(a) and 6(c)). These are due to the tip leakage flow, moving from the suction side of one blade to the pressure side of the adjacent blade, and representing a major part of losses in a rotor. At off-design conditions, a structure of high entropy, circled in white, clearly appears in Fig. 6(d). It extends over almost three rotor passages in the circumferential direction, and from mid-chord of rotor blade to mid-chord of downstream stator vane. It is similar to previous URANS results (Crevel et al., 2014) and seems to match the definition of the expected rotating instability. Such a structure is not really identified for grid M1, probably due to the lack of grid resolution in the rotor 3 tip clearance. Hence the following analysis focuses on grid M2 only.

In a turbomachinery flow, an instantaneous variable such as the pressure  $P$  can be decomposed into spatial Fourier series in the circumferential direction  $\theta$ , such as:

$$P(\theta, t) = \sum_m \hat{P}_m(t) e^{im\theta}, \quad \text{with} \quad \hat{P}_m(t) = \frac{1}{2\pi} \int_0^{2\pi} P(\theta, t) e^{-im\theta} d\theta. \quad (4)$$

In the simulation, the integration of Eq. (4) is performed only over the azimuthal sector. Figure 7 corresponds to modal coefficients  $\hat{P}_m$  of pressure recorded at 83%  $h/H$  between R3 and S3, for grid M2 at off-design conditions. These data are plotted over one rotor revolution (80 R3 blade passing periods). Several bands centered around given spatial modes can be distinguished. For most of them, these azimuthal modes are created by rotor-stator interactions (RSI). According to Tyler and Sofrin (1962), the pressure field resulting from RSI can be decomposed into circumferential modes of order  $m_{RSI}$ , such as:

$$m_{RSI} = \sum_j a_j N_{R,j} + b_j N_{S,j}, \quad (a_j, b_j) \in \mathbb{Z}^2, \quad (5)$$

where  $N_{R,j}$  and  $N_{S,j}$  are the number of rotor blades and stator vanes of stage  $j$ . In Fig. 7, a band

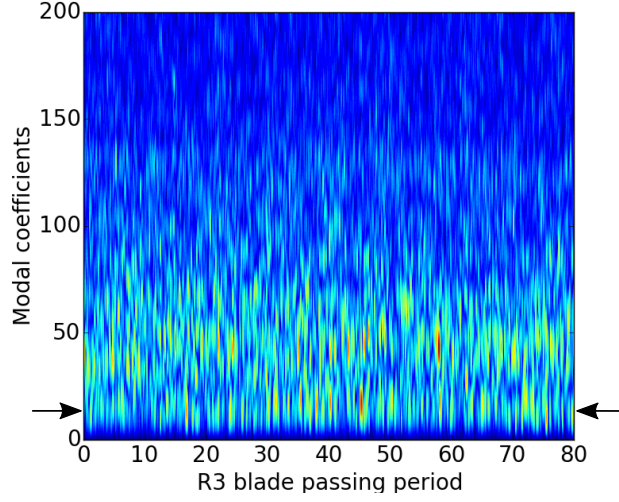


Figure 7: **Azimuthal modal coefficients of pressure, at 83% h/H, between R3 and S3, for M2 grid. Normalized color scale varies from 0 (blue) to one (red).**

centered around the mode 16, indicated by arrows, is present whereas this value is not a possible solution of Eq. (5). This mode, not generated by RSI, indicates thus the rotating instabilities. Together with Fig. 6(d), this confirms that 16 instabilities around the annulus are present at 83% h/H, i.e. one instability for the simulated sector of  $2\pi/16$ .

So far, the spinning velocity of rotating instabilities could not be determined. In a multistage compressor, RSI frequencies are precisely known, and can be expressed as:

$$f_{m_{RSI}} = \sum_j a_j N_{R,j} f_{shaft}, \quad (6)$$

where  $f_{shaft}$  is the rotational frequency of the shaft, while  $a_j$  and  $N_{R,j}$  are defined for Eq. (5). Figure 8 compares pressure spectra, locally recorded at 83% h/H between R3 and S3, at nominal and off-design conditions. Frequencies are normalized by  $f_{shaft}$ . The RSI frequencies clearly appear from the spectra, and correspond to the blade passing frequency (BPF) of R1 (64), BPF of R2 or R3 ( $BPF_{R23}$ ) (80), a combination of  $BPF_{R1}$  and  $BPF_{R23}$  (144), and the first harmonic of  $BPF_{R23}$  (160). At off-design,  $BPF_{R1}$  is not present in the spectrum, and amplitudes of frequencies 144 and 160 are lower than at nominal point. This suggests a more perturbed pressure field at off-design. Moreover, an additional frequency content is present in the red curve, circled in blue. This could represent the trace of the rotating instabilities passing at this location. To determine more precisely their frequency, a more advanced post-processing treatment such as the Dynamic Mode Decomposition (DMD) is needed. This technique has already been used to identify particular modes at off-design conditions, by Semlitsch and Mihaescu (2016) for instance. The principle of DMD consists in decomposing a field into modes, each one having a particular frequency, an amplitude and an amplification. This technique allows determining the most energetic modes existing in the flow, since a high value for the amplitude indicates a mode with significant energy provided that its amplification is not too low. The DMD has been applied on the entire interface plane between R3 and S3 over almost one compressor rotation. As it could be expected, the most energetic mode given by this decomposition, using the entropy variable, corresponds to the 53<sup>th</sup> mode at the frequency  $BPF_{R23}$ . The 7<sup>th</sup> mode also presents a

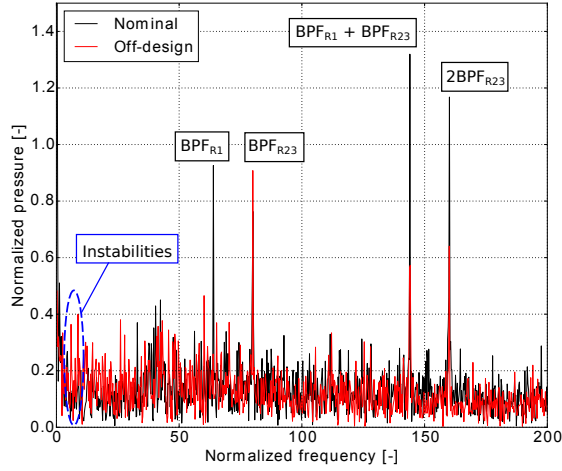


Figure 8: **Pressure spectra recorded between R3 and S3, at 83% h/H, in M2 grid. Frequency is normalized by shaft frequency.**

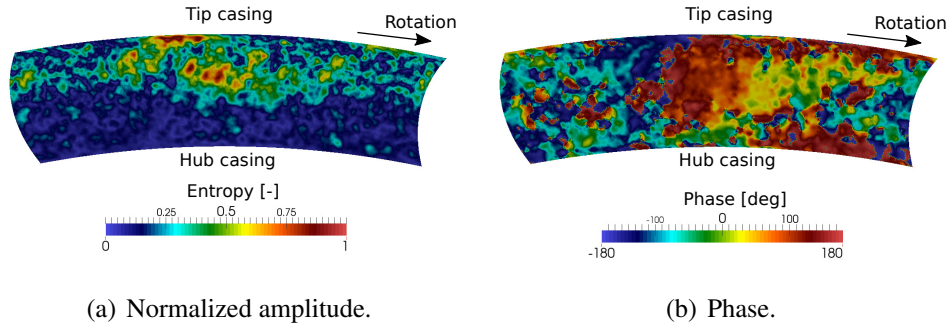


Figure 9: **Mode 7 of the Dynamic Mode Decomposition on entropy, at 1840 Hz, between R3 and S3, for M2 grid.**

significant amplitude, its frequency being 1840 Hz. The amplitude and phase of the entropy corresponding to this mode are shown in Fig. 9. This figure highlights a single structure of high entropy value, located between 50 and 90% of the duct height and having a width of around 3 S3 vane passages. This structure clearly corresponds to a rotating instability, given its location, its amount (one per sector) and its frequency  $f_i = 1840$  Hz, within the range identified in Fig. 8. Since  $m_i = 16$ , instabilities present around the annulus have a spinning velocity following:

$$\Omega_i = \frac{1}{m_i} \frac{f_i}{f_{shaft}} \Omega_{shaft}, \quad (7)$$

i.e. around 60% of shaft speed. This study is found to be in correct agreement with experimental observations, that have highlighted 18 rotating instabilities at 57% of shaft speed (Courtiade and Ottavy, 2013). URANS data from Crevel et al. (2014) showed 24 structures at 79.2% of shaft speed in the isolated compressor, and 16 rotating instabilities at 80.6% in the full test rig configuration. This is still in agreement with the current LES, even if the spinning velocity is slightly larger than both experimental and LES results.

## CONCLUSIONS

This work has attempted to evaluate the relevance of wall-modeled LES applied to an actual high pressure multistage compressor at off-design conditions. A coarse and an intermediate grid were used, the latter fulfilling accepted criteria for near wall resolution on blades in a wall law context. If both grids are shown to reproduce the shape of the iso-speed performance line of the compressor, only the intermediate grid satisfactorily approaches the experimental operating point corresponding to the lowest mass flow. Hence this grid resolution seems to appear sufficient for global performance predictions. For both grids, the last stage is found to be unstable, as previously observed in this compressor in experimental and numerical investigations. In LES, the flow field evolution between nominal and off-design conditions has been analyzed in terms of velocity fluctuations and instantaneous entropy. For the intermediate grid, the expected flow behavior is qualitatively observed, e.g. flow separation on suction surfaces of stator vanes and tip leakage flow pushed towards the inlet of rotor passages. Furthermore, rotating instabilities have been evidenced in the intermediate grid at off-design conditions, above the duct mid-height. More specifically, 16 structures spinning at around 60% of shaft speed have been highlighted. This amount is enforced to be a multiple of the circumferential periodicity, but is close to experimental observations, in which 18 rotating instabilities were measured at 57% of shaft speed. Some comparisons performed with existing URANS results of the same compressor are also satisfactory, in terms of global performance predictions and rotating instabilities in the last stage. Finally relatively coarse wall-modeled LES appears to be promising as an acceptable tradeoff between global flow predictions and computational cost. Complemented by DMD, it is also found to be an efficient technique to identify instabilities at off-design conditions. Further evaluations are still required to assess these conclusions. Coupling a two-variable outlet condition to the current characteristic condition could also be an interesting perspective for future simulations of unstable regimes.

## ACKNOWLEDGEMENTS

This work was granted access to the HPC resources of CINES under the allocation x20162a-6074 made by GENCI. The authors are grateful to X. Ottavy and J. Schreiber (LMFA) for fruitful discussions on CREATE.

## References

- [1] N. Courtiade and X. Ottavy. Experimental study of surge precursors in a high-speed multistage compressor. *J. Turbomach.* , 135, 2013.
- [2] F. Crevel, N. Gourdain, and S. Moreau. Numerical simulation of aerodynamic instabilities in a multistage high-speed high-pressure compressor on its test rig - part I: rotating stall. *J. Turbomach.* , 136, 2014.
- [3] I. J. Day. Stall, surge and 75 years of research. *J. Turbomach.* , 138, 2016.
- [4] J. de Laborderie, F. Duchaine, O. Vermorel, L. Gicquel, and S. Moreau. Application of an overset grid method to the Large Eddy Simulation of a high-speed multistage axial compressor. In *ASME Turbo Expo*, number GT2016-56344, 2016.
- [5] F. Duchaine, S. Jauré, D. Poitou, E. Quémerais, G. Staffelbach, T. Morel, and L. Gic-

- quel. Analysis of high performance conjugate heat transfer with the OpenPALM coupler. *Computational Science & Discovery*, 8(1):15003–15021, 2015.
- [6] C. Koupper, T. Poinso, L. Gicquel, and F. Duchaine. Compatibility of characteristic boundary conditions with radial equilibrium in turbomachinery simulations. *AIAA Journal*, 52(12):2829–2839, 2014.
- [7] P. D. Lax and B. Wendroff. Difference schemes for hyperbolic equations with high order of accuracy. *Commun. Pure Appl. Math.*, 17:381–398, 1964.
- [8] V. Moureau, G. Lartigue, Y. Sommerer, C. Angelberger, O. Colin, and T. Poinso. Numerical methods for unsteady compressible multi-component reacting flows on fixed and moving grids. *J. Comput. Phys.*, 202(2):710–736, 2005.
- [9] X. Ottavy, N. Courtiade, and N. Gourdain. Experimental and computational methods for flow investigation in high-speed multistage compressor. *J. Prop. Power*, 28(6):1141–1155, 2012.
- [10] T. Poinso and S. Lele. Boundary conditions for direct simulations of compressible viscous flows. *J. Comput. Phys.*, 101(1):104–129, 1992.
- [11] T. Schonfeld and M. Rudgyard. Steady and unsteady flows simulations using the hybrid flow solver AVBP. *AIAA Journal*, 37(11):1378–1385, 1999.
- [12] J. Schreiber, X. Ottavy, G. Ngo Boum, and N. Gourdain. Influence of rotor tip flow field mis-prediction on rotating disturbance near surge in a high speed multistage compressor. In *ASME Turbo Expo*, number GT2016-57372, 2016.
- [13] B. Semlitsch and M. Mihaescu. Flow phenomena leading to surge in a centrifugal compressor. *J. Energy*, 103(572–587), 2016.
- [14] J. Smagorinsky. General circulation experiments with the primitive equations: 1. the basic experiment. *Mon. Weather Rev.*, 91:99–164, 1963.
- [15] P.G. Tucker. Computation of unsteady turbomachinery flows: Part 2 LES and hybrids. *Prog. Aerospace Sci.*, 47(7):546 – 569, 2011.
- [16] J. Tyler and T. Sofrin. Axial flow compressor noise studies. *SAE Technical paper 620532*, 1962.
- [17] M. Vahdati, A. Sayma, C. Freeman, and M. Imregun. On the use of atmospheric boundary conditions for axial flow compressor stall simulations. *J. Turbomach.*, 127(2):349–351, 2005.
- [18] G. Wang, F. Duchaine, D. Papadogiannis, I. Duran, S. Moreau, and L. Y. M. Gicquel. An overset grid method for large eddy simulation of turbomachinery stages. *J. Comput. Phys.*, 274:333–355, 2014.